EFFECT OF TRAILING EDGE DAMAGE ON FULL-SCALE WIND TURBINE BLADE FAILURE

Philipp U. Haselbach[1] and Kim Branner[1]
[1]Department of Wind Energy, Technical University of Denmark
P.O. Box 49, Frederiksborgvej 399, DK-4000 Roskilde, Denmark
Email: phih@dtu.dk, web page: http://www.vindenergi.dtu.dk/

Keywords: Adhesive joints, Crack propagation, Fracture mechanics, Trailing edge damage, Wind turbine blade

ABSTRACT

Modern wind turbine rotor blades are normally assembled from large parts bonded together by adhesive joints. The structural parts of wind turbine blades are usually made of composite materials, where sandwich core materials as well as fibre composites are used. For most of the modern wind turbine blades the aerodynamically formed outer shell structure is manufactured as an upper and a lower part in separate moulds in order to simplify the production process. The aerodynamic shell structures are then bonded to internal load bearing structures during the production process. Adhesive joints exist where the load bearing structure is connected to the shells and at the joints of the upper and lower shells, usually at the leading and trailing edges. Maintenance inspections of wind turbines show that cracks in the vicinity of the trailing edge are typically occurring forms of damage. The cause of trailing edge failure is very complex and can arise from manufacturing flaws, damages during transportation and erection as well as under general and extreme operational conditions.

The focus in this study is put on the geometrical nonlinear buckling effect of the trailing edge under combined loading and how it affects the ultimate strength of a holistic blade. For this reason a 34m long blade was studied experimentally and numerically under ultimate load until blade collapse. The interaction between trailing edge buckling on damage onset and sandwich panel failure was studied in detail. Numerically applied fracture mechanics approaches showed good agreement with the experimental results and helped to understand the relations between trailing edge buckling and blade collapse.

1 INTRODUCTION

Rotor blade issues constitute with approximately 2% to 5% to the annual failure rate of wind turbines but cause 8% to 20% of the total downwind time of wind turbines according to a NREL report [1]. In average 2% of wind turbines per year during the first 10 years operational period require blade replacements. Blade replacements in the first two years of operation are typically caused by manufacturing defects or damages originated during transport and erection [1]. Rotor blades see increased failure rates or reduced reliability as the concept goes from simple design concepts (simple Danish concept) with small rotor diameters towards more advanced technologies with bigger rotor span [1].

Inspection reports and technical papers such as Ataya and Ahmed [2] indicate that trailing edge failure is frequent observed for rotor blades. The cause of trailing edge failures is complex and often results as a combination of complex loading conditions, anisotropic material behaviour, complex geometries, manufacturing process and blade design. Non-linear geometry effects and their impact on the trailing edge have been studied in [2, 3, 4, 5]. The effect of bondline shapes was investigated by Eder and Bitsche [6].

Often simplified methods like slice approaches, linear Beam Cross Section Analysis Software (BECAS) [7] or similar methods are used. The methods are computational efficient but have the

disadvantage of neglecting the holistic view. In order to understand the stresses and strains occurring under complex loading and to predict the blade response accurately, detailed structural modelling with Finite Element Methods (FEM) of the entire wind turbine blades has to be conducted. This approach can be computational expensive. Often shell element models are used to model blades. But does this method allow accurate predictions of trailing edge failures? And how can trailing edge failure be included without huge modelling afford but still representing damage mechanics sufficiently?

In this study an answer is given on how a simplified trailing edge model can predict the effect of damage in the trailing edge and on how this damage affects the response of the wind turbine blade structure under ultimate loading. Therefore, numerical studies were compared to experimental findings.

2 METHODS

2.1 Experimental setup

DTU Wind Energy tested 3 wind turbine rotor blades of the 1.5MW class with an original length of 34m. The blade tip was truncated at a radial position of 29.5m to a fit into the blade testing facility at DTU Risø Campus. The blade root was bolted to an adapter ring under a pitch angle of -30º. The adapter and so the blade axis featured an angle of 8º in order to increase the distance between blade tip and floor. Four curved anchor steel plates with an approximately size of 0.4m x 0.4m x 0.015m were glued to blade on the suction-side cap and acted as load points (LPs). Pulleys were connected to the adhesively connected anchor plates. The blade was loaded by means of displacement controlled winches pulling steel cables running through the pulleys towards the floor (see Figure 1).

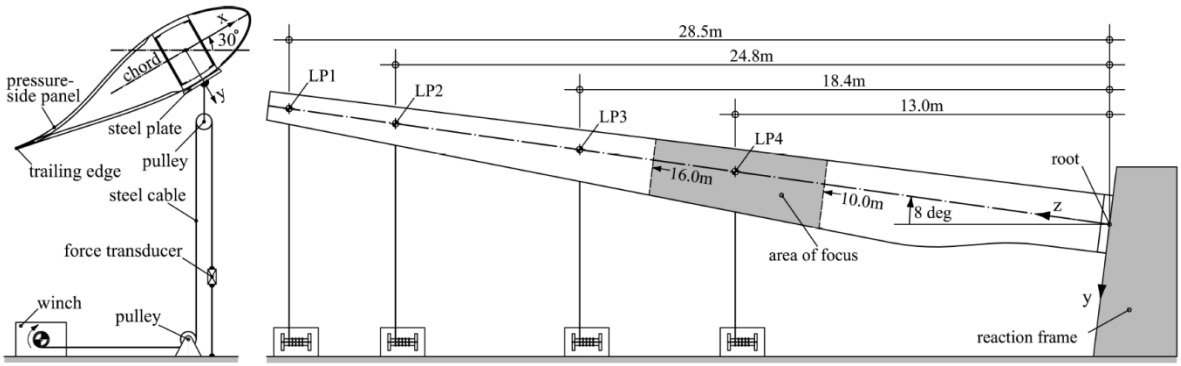

Figure 1: Sketch of the experimental test setup [taken from Haselbach et. al. [5]].

The blade was loaded by pulling incrementally at all load points at a low rate of ≤ 0.1m min^{-1} leading to a quasi-static load. The blade deflection was measured by the use of linear cable position sensors of type ASM HBM Posiwire 6250 (ASM). Four ASMs measuring the global blade displacement between suction side cap and floor long the radial blade position of z=10.0m, z=16.0m, z=22.0m and z=29.0m were installed.

The trailing edge displacement between 10.0m and 16.0m radial position was measured by means of an optical displacement measurement camera system and two additional ASMs attached to the trailing edge at 10.0m and 16.0m. The optical displacement measurement system is an in-house stereo photogrammetry tracking the 3D displacement of marker points along the trailing edge described more in detail in [5].

2.2 Applied loads and aero-elastic simulations

A bending moment distribution corresponding to the bending moment distribution extracted from aero-elastic simulation was applied. The load ratio for the individual LPs are given in Table 1.

		LP1	LP2	LP3	LP4
Distance	[m]	28.50	24.80	18.40	13.00
Load ratios	[-]	1.000	0.937	0.775	0.775

Table 1: Locations and target load ratio for the four load points (LPs).

The loads applied at the LPs leading to the maximum bending moment under which the blade collapsed is defined as the reference loads. The load ratios are calculated by normalising these with the reference loads.

Aero-elastic simulations with the DTU owned software package HAWC2 version 11.9 (Horizontal Axis Wind turbine simulation Code 2nd generation [8, 9]) were conducted to benchmark the ultimate load of the blade. All relevant Design Load Cases (DLCs) according to IEC 61400-1 [10] were computed in order to predict the design load. The blade airfoil geometry and cross section stiffness properties of the blade were used together with an available Neg Micon NM80 turbine. Originally, the NM80 was designed for a rated power of 1.75 MW to 2.5 MW. The wind turbine model of the NM80 was chosen due to similar blade lengths of 38.8m. The turbine model was down-rated to 1.5 MW and its controller setup adjusted accordingly. The controller was fitted by means of the aero-elastic-servo-elastic stability tool HAWC2Stab2 [11]. The extreme loads include the DLCs corresponding safety factors. The bending moments for cross sections along the blade span for a load direction of -30º were evaluated and the highest magnitudes picked. From each individual cross section a bending moment distribution for the blade for the given angle could be determined. The procedure and chosen model was considered to be suitable as a benchmark to the experimentally determined ultimate load.

2.3 Numerical model and approaches

For the Finite Element Analysis Abaqus version 13.9 [12] were used. The blade geometry was discretized with 67,000 8-node doubly curved thick shell elements with reduced integration (Abaqus type S8R) with a characteristic element length of approximately 0.05m. The adhesive bondline at the trailing edge between the upper and lower aero-dynamic shell was modelled by the use of 8-node linear brick elements with reduced integration and hour glass control (Abaqus type C3D8I). This modelling approach was used in order to easily apply different fracture mechanics approaches to the trailing edge. The adhesive of the trailing edge starting at a radial position of 8m to the end of the truncated blade at 29.5m was modelled with a bondline width of 0.08m. Different degrees of discretization depending on the chosen fracture mechanic model were used in order to balance accurate prediction and computation time. The finest discretization was based on 275,000 8-node linear brick elements discretising the geometry with fours layers of elements through the thickness and a characteristic element length of 0.005m. The roughest discretization had 120,000 8-node linear brick elements with only two layers of elements with a characteristic element length of 0.01m. The solid brick elements were connect by means of tie-constraints to the shell elements as shown in Figure 2.

All degrees of freedom in the central node at the blade root were restrained and transferred via a kinematic (rigid) coupling constraint assigned to the nodes at the blade root circumferences. Besides gravity loading, the blade was loaded force-controlled by means of four axial connector elements (see Figure 3). Four load introduction points (LPs) acted as master nodes for rigidly connected nodes representing the anchor plates placed at the cap along the suction side. Axial connector elements connected the master nodes of the four individual LPs at the blade with the referring reference points at the rigid floor (see Figure 4). The connector elements were chosen due to the advantage that the applied force is axial aligned with the connector elements. Thus, the model represented more realistically the experimentally applied loading conditions in conjunction with the large blade deformation.

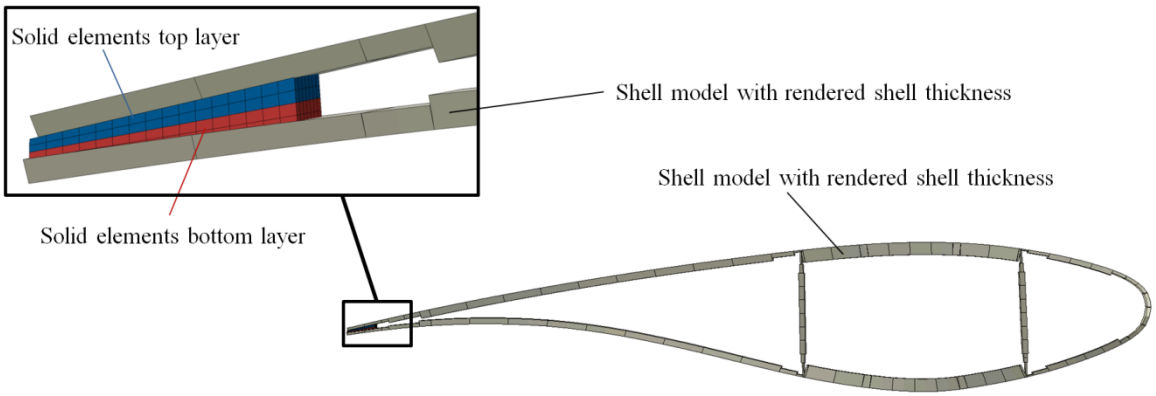

Figure 2: Wind turbine blade model cross section with rendered shell elements and solid elements in the trailing edge. The solid elements are tied to the shell elements with tie-constraints.

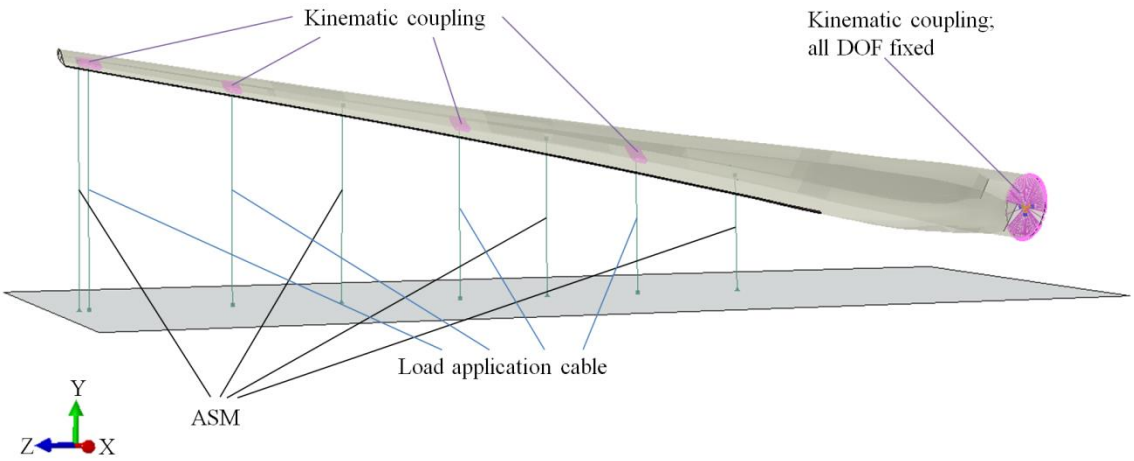

Figure 3: Boundary conditions of the blade model.

The numerical analysis was executed as a quasi-static geometric non-linear analysis. A dynamic implicit solver was chosen. The loads were slowly ramped up, thus the kinematic energy level could be neglected and a quasi-static performance was reached.

Different failure criteria and fracture mechanic models were applied to the model in order to capture relevant parameters and to model progressive damage and failure. Maximum strain, maximum stress, Tsai-Hill, Azzi-Tsai-Hill and Tsai-Wu failure theories were used for a primarily failure prediction, whereas, the Hashin criterion [13, 14, 15, 16] and cohesive element methods were used for more detailed progressive damage and failure simulation [17, 18]. The Virtual Crack Closure Technique (VCCT) was used to extract nodal forces and the relevant strain energy release rate ratio (SERR) along the trailing edge [12, 19].

The maximum strain and maximum stress failure criteria are very simple criteria. Failure occurs when any of the strain or stress components in the principal material axes exceed the corresponding critical value. The components are independently judged and the failure envelope is a rectangle. For the maximum strain criteria an interaction of stresses based on the Poisson´s effect is given and the failure envelope is a parallelogram.

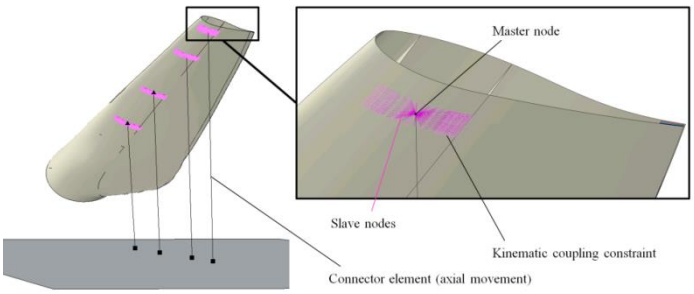

Figure 4: Kinematic coupling constraints acting as anchor plates and load introduction for the applied transversal forces.

The Tsai-Hill, Azzi-Tsai-Hill and Tsai-Wu are quadratic, orthotropic plane stress failure criteria normally used for fiber-reinforced composite materials. These criteria calculate an equivalent stress and make an attempt to take account of interactions in a multi-axial stress state. The failure envelopes are ellipses.

The Hashin criterion is a progressive damage and failure theory for elastic-brittle materials with anisotropic behavior, like e.g composite materials. The progressive failure theory is based on two steps. Firstly, a failure criterion is evaluated for each lamina individual and at each load step. If a lamina exceeds the critical value, the lamina is considered as failed and its stiffness is reduced and the entire stiffness matrix has to be recalculated. This progressive damage calculation can be repeated until ultimate failure is reach and the structure fails [13, 14, 15, 16].

Surface-based cohesive behavior allows simulating debonding processes of interfaces. The cohesive behavior is based on a linear elastic traction-separation law. The approach allows crack growth and debonding of the adhesive bondline at the trailing edge. Two different scenarios had been considered. One with the manufacturer specific bondline material properties of the adhesive (fracture toughness = Kc = 3.55 MPa, G_{Ic} = 4400J/m^2, G_{IIc} = G_{III} = 5460 J/m^2) and another one with a reduce fracture toughness of approximately 80% of the original strength. The reduced fracture toughness was considered in order to take account for expected flaws in the bondline as detected by ultrasound scanning for a similar blade described in Eder et al. [6]. For the model and the failure theories the material properties given in Table 2 were used. The fracture energies for all laminates were set to 1200 J/m^2 for Mode I and 4000J/m^2 for Mode II and Mode III according to [20].

Engineering constant		U/D Glass	Triaxial Glass	Triaxial Glass (HRC)	Biaxial Glass	Biaxial Glass (Pre-preg)	Polymer Foam
E_1	[GPa]	41.26	20.26	16.67	12.75	11.58	0.0485
E_2	[GPa]	11.39	10.42	8.587	12.75	11.58	0.0485
ν_{12}	–	0.33	0.50	0.50	0.50	0.50	0.40
G_{12}	[GPa]	3.91	7.35	6.605	10.06	10.06	0.0391
$\boldsymbol{\varepsilon}_{\text{tensile}}$	–	0.021	0.023	0.023	0.017	0.011	-
$\boldsymbol{\varepsilon}_{\text{compressive}}$	–	0.016	0.012	0.016	0.015	0.014	-
$\boldsymbol{\varepsilon}_{\text{shear}}$	–	0.0037	0.014	0.014	0.014	0.014	-
X^T	[MPa]	90.00	47.21	38.90	21.42	12.39	0.14
X^C	[MPa]	66.00	32.42	26.72	18.49	15.63	0.14
Y^T	[MPa]	42.14	12.71	10.48	18.49	15.63	0.14
Y^C	[MPa]	42.14	12.71	10.48	18.49	15.63	0.14
S^L	[MPa]	58.65	9.925	8.917	14.39	14.39	0.14
S^T	[MPa]	58.65	9.925	8.917	14.39	14.39	0.14

Table 2: Material properties: longitudinal modulus E_1, transverse modulus E_2, Poisson´s ratio ν_{12} shear modulus G_{12}, allowable tensile strain $\boldsymbol{\varepsilon}_{\text{tensile}}$, allowable compressive strain $\boldsymbol{\varepsilon}_{\text{compressive}}$, allowable

shear strain $\boldsymbol{\varepsilon}_{shear}$, longitudinal tensile strength X^T, longitudinal compressive strength X^C, transverse tensile strength Y^T, transverse compressive strength Y^C, longitudinal shear strength S^L and transverse shear strength S^T. Triaxial is a triaxial glass fibre fabric and Triaxial 2 is a triaxial glass fibre fabric too, but contains higher amount of resin (high resin content = HRC). UD represents unidirection glass fibre cloths, Biaxial Pre-preg represents biaxial glass fibre pre-preg cloths, whereas Biaxail is a sprint biaxial glass fibre cloth and Glue represents the epoxy-based bonding paste used for the joints.

3 RESULTS

3.1 Aero-elastic loads and ultimate load

The maximum design load based on the conducted aero-elastic simulation for the blade, at the load direction shown in Figure 1, led to approximately 90% of the experimentally found ultimate load, at which the blade collapsed under the experimental testing.

During testing initial blade damage occurred at approximately 90% of the ultimate load. This resulting bending moment corresponds to the range of the ultimate design load (including safety factor) of the blade under the specific load angle considering all relevant DLCs.

Figure 5a shows the corresponding load levels normalised to 1.

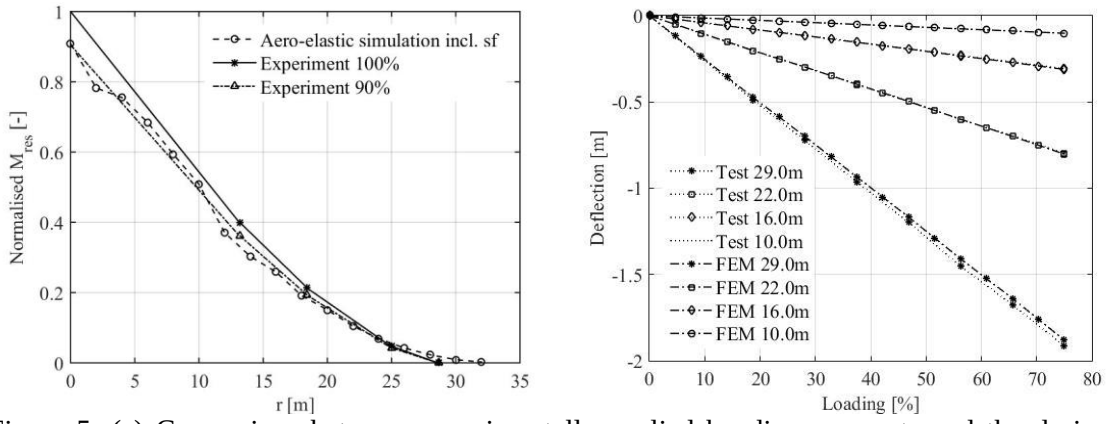

Figure 5: (a) Comparison between experimentally applied bending moments and the designated maximum design load determined by aero-elastic load analyses (left). (b) Comparison between experimentally measured displacements by means of ASM and numerical results (right).

3.2 Model validation

Before conducting an ultimate test, the blade was loaded up to approximately 75% of the ultimate load. This test was used to validate the accuracy of the numerical blade model. The global blade response measured by means of the ASM installed at radial positions of 10.0m, 16.0m, 22.0m and 29.5m, was compared to numerical results. The comparison showed an excellent agreement between the numerical and experimental results as shown in

Figure 5b and Table 3. The maximum deviation for the global displacement was less than 2% at the blade tip.

Radial position	[m]	z=29.5	z=22.0	z=16.0	z=10.0
ASM	[m]	-1.914	-0.797	-0.307	-0.102
Numeric	[m]	-1.880	-0.802	-0.311	-0.102
Deviation	[%]	-1.77	0.62	1.38	0.00

Table 3: Experimental (ASMs) and numerically obtained global deformation at 75% of the reference load.

3.2 Nonlinear simulation results without progressive damage mechanic modelling

In Figure 6a the global displacement of the trailing edge measured with the optical displacement measurement camera system between at radial position of 12m to 16m is plotted in comparison to numerically predicted displacements. Clearly the onset of nonlinear geometric deformation of the trailing edge can be seen for loads above 75% of the ultimate load. In order to visualize the buckling onset a 4th order polynomial curve fit following the global displacement of the entire trailing edge is plotted as a dash line for the numerical results. Subtracting the global displacement from the course of the 4th order polynomial curve fit led to the Δu_y shown in Figure 6b**.** The local trailing edge deformation showed a distinct increase in magnitude when the load was raisen from 67% to 76%. Here, the numerical prediction differs from the experimentally gained data. The numerical model underestimates the magnitude of the buckle slightly. Interesting is also that the deformation seems to move slightly with increasing load. For the experimental obtained displacement the buckling wave is moving slightly towards the blade tip for increased loads while it moves towards the root for the numerical results. This means that even though the position of the buckling wave agrees well at low load level, this is not the case at higher load level where they move further apart.

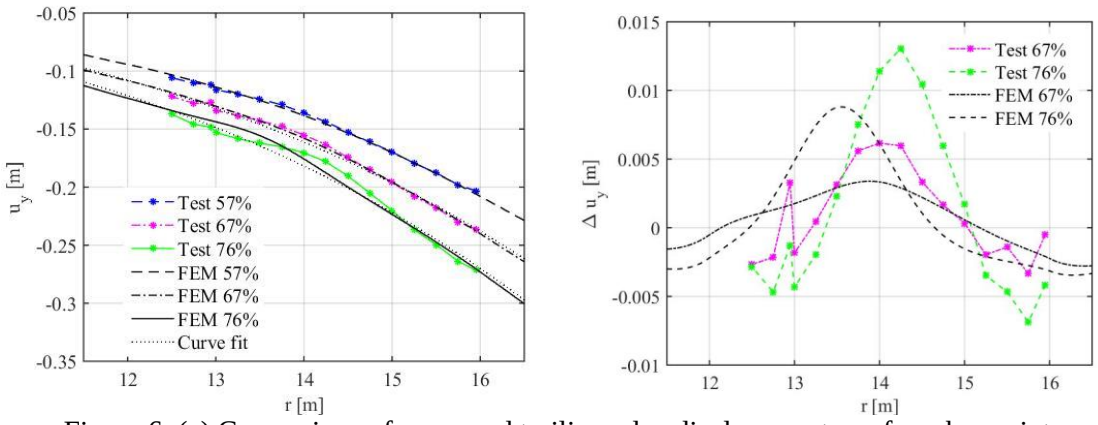

Figure 6: (a) Comparison of measured trailing edge displacement u_y of marker points and numerical displacement results (left). (b) Comparison of local deformation as offset from a curve fit through the global displacement (right).

With increasing load level the buckling wave formation became more distinct as shown in Figure 7a. In general, the numerical simulation differed from the experimental results in buckling peak location and buckle wave magnitude. The magnitudes of numerical model are less marked compared to the measured local deformation and their position is offset by approximately 1m radial position at failure.

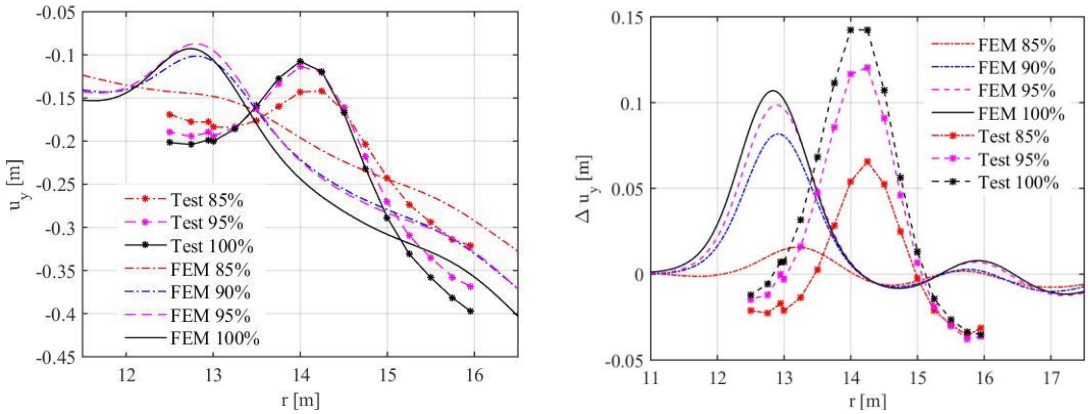

Figure 7: (a) Comparison of measured trailing edge displacement u_y of marker points and numerical displacement results (left). (b) Comparison of local deformation as offset from a curve fit through the global displacement (right).

The reason for the differences in magnitude was found in a damage onset in the vicinity of the trailing edge under experimental testing. The trailing edge buckling caused kinking of the sandwich panel. In the numerical model without progressive damage and failure implementation, the damage was predicted but had no stiffness degradation effects on the structure. The experiments showed a distinct kink in the trailing edge panel on pressure side whereas the model showed high stresses without kinking. With increased load the kink became more distinct as shown in Figure 8.

Figure 8: Trailing edge deformation just before reaching the ultimate load (right). Note the distinct kink at the upper surface.

The nonlinear simulations without progressive damage mechanic predicted ply failure for load levels between 90% and 100% of the ultimate load. The ply failure was predicted in the sandwich structure forming the trailing edge panel in the vicinity of the buckled trailing edge. Depending on the applied failure criteria, the failure was predicted for different load levels as given in Table 4. The stress-based failure theories were more conservative than the Maximum strain criterion. The most conservative criterion was the Tsai-Wu failure criterion predicting ply failure at a load level of approximately 90% of the ultimate load. Max stress, Tsai-Hill, Azzi-Tsai-Hill predicted ply failure around a load level of 95%. The maximum stress criterion predicted failure at ultimate load.

Failure criterion	[-]	Tsai-Wu	Tsai-Hill	Azzi-Tsai-Hill	Max stress	Max strain
Load level	[%]	90	95	95	95	100

Table 4: Failure criteria and referring load level.

Obviously the trailing edge buckle caused damage in the sandwich composite panel at the pressure side. According to Zenkert [21] there exist different failure modes for sandwich panels. The sandwich panel at the pressure side was due to the deformation bended and loaded in compression and started to kink. The load configuration prevailed in the vicinity of the kinked sandwich composite panel corresponded to failure mode face wrinkling, where the skin buckles. Final failure of the sandwich face usually leads to crushing of the core. The failure mode typically occurs for thin skin sandwich structures with relatively low-density core material as used for wind turbine blades. Also the failure mode map present by Triantafillou and Gibson [22] indicates wrinkling as the failure type. The face sheet thickness (h_f) to span length (L) ratio is approximately $h_f/L = 0.002$ and the core relative density, $\rho_c/\rho_u = 0.06$ (ρ_c =density of the foam material, unfoamed, ρ_u = solid material properties of the foam base material).

3.2 Nonlinear simulation results progressive damage mechanic modelling

In order to consider the sandwich panel damage and its impact on the blade stiffness Hashin´s progressive damage and failure theory was applied to the blade structure. Hashin´s theory predicted at a load level of approximately 85% a combination of shear and compressive matrix damage initiation and damage propagation in outer skin layers of the composite material forming the suction side panel as shown in Figure 9. Shortly after, the core material crushed under a combination of shear and compression failure.

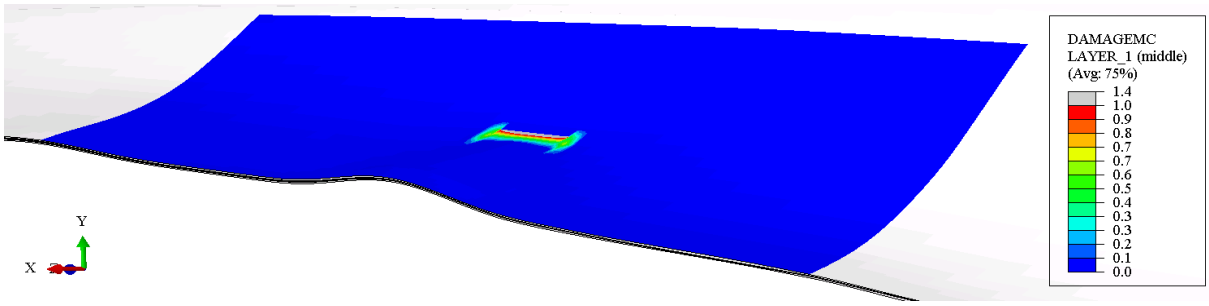

Figure 9: Hashin´s compressive matrix damage critierion. The gray marked area indicates ply failure in the outer most skin layer of the suction side at a load level of 85%.

The applied progressive damage and failure theory affected the response of the numerical model. The trailing edge deformation became more pronounced in magnitude (see Figure 10a). The numerical results now show very good agreement with the magnitude of the measured trailing edge displacement u^y and Δu^y as shown in Figure 10b.

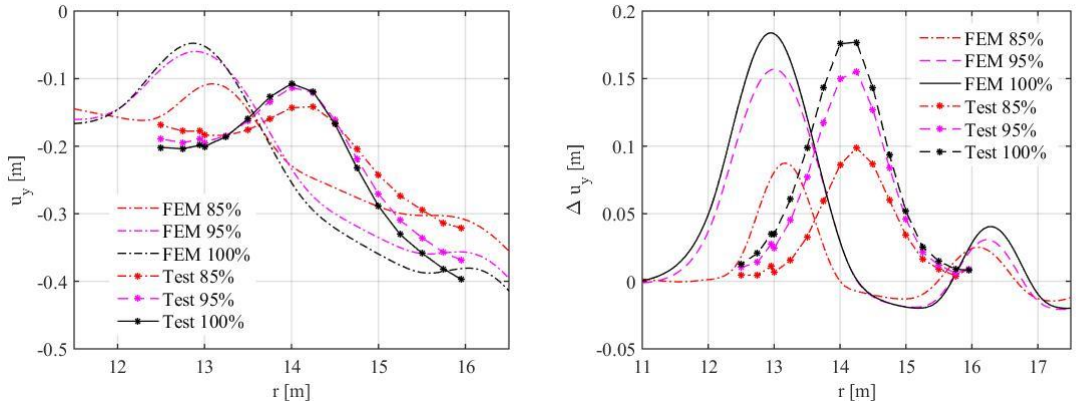

Figure 10: (a) Comparison of measured trailing edge displacement u_y of marker points and numerical displacement results (left). (b) Comparison of local deformation as offset from a curve fit through the global displacement (right).

The higher the loads, the more prone is the trailing edge buckling and the progressive damage in the sandwich panel grows. This finally had a significantly effect on the bondline in the trailing edge. The buckling wave had a big impact on the local stress and strain ratio acting at the bondline and changed this with increase buckling wave magnitude. In order to determine the strain energy release rate (SERR) at the bondline a small crack in the middle of the adhesive glue was simulated and the SERR calculated. The SERR increased significantly at a load level of approximately 85%, when sandwich failure in the vicinity of the trailing edge onset (see Figure 11). The mode-mixity changed from an opening mode (Mode I) to a shear dominated mode (Mode III). Looking the Finite Element Analysis the buckled trailing edge had its maximum at a radial position of around 13.0m. The buckling wave forced the upper and lower trailing edge panels in a state, where they were closing and the shear stress dominated. Accordingly, G_{III} was dominating the mode-mixity. The stress concentration in the trailing edge increased with increasing load as shown in Figure 11 and calculated with the following Equation (1) and (2)

$$G_{tot} = G_I + G_{II} + G_{III} \quad (1)$$

$$G_{equ} = G_{Ic} + (G_{IIc} - G_{Ic}) * ((G_{II} + G_{III})/G_{tot})^{\lambda} \quad (2)$$

where G_{tot} is the total energy, G_I, G_{II} and G_{III} are the strain energy releases rates for Mode I, Mode II and Mode III, respectively. G_{ic} determines the critical energy release rates and G_{equ} is the equivalent

energy release rate. The exponent λ describes the interaction between the mode-mixity and depends on the resin type (λ= 2 for brittle resins and λ= 3 for ductile resins) [6].

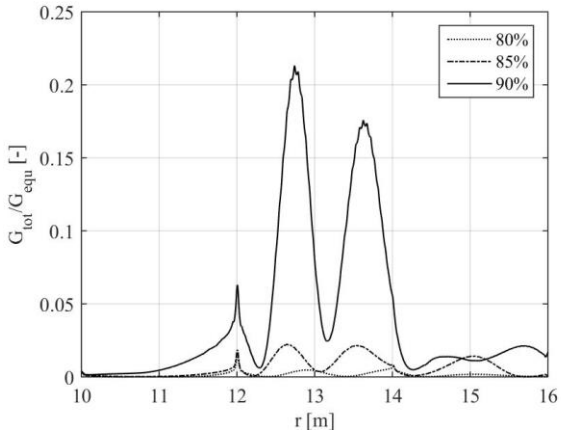

Figure 11: G_{tot}/G_{equ} as function of the radial blade position.

In the numerical prediction with the reduced fracture toughness, the critical damage initiation stress is satisfied at a load level of 85% of the experimentally determined ultimate load and damage initiation therefore started in the trailing edge. Only a small initial crack started which did not separate the bondline completely. At that load level of 97.5% the crack propagated and the energy in the trailing edge G_{equ} exceeded the critical energy level G_C, which led to a sudden trailing edge failure (see Figure 12). The numerically predicted failure mode is in agreement with the recorded failure mode during the test.

9 DISCUSSION AND CONCLUSIONS

The conducted study showed how the interaction between trailing edge and sandwich panel failure led to blade collapse. The chosen numerical modelling approach showed accurate trailing edge failure prediction. By applying the Hashin´s progressive damage and failure theory, sandwich failure could be predicted, which improved the accuracy significantly. The modelling approach seems to be suited for accurate numerical fracture prediction in combination with the applied fracture mechanical approaches.

The uses of Hashin´s degradation progressive damage and failure theory was computational expensive and only applied in order to understand the entire fracture process that occurred during testing. This computational expensive method is not necessary to implement for design processes since the sandwich panel damage was a successive failure caused by prone trailing edge buckling. The trailing edge buckling should be considered as the primary failure. The primary failure could to some extend be predicted with the simple failure criteria by means of running a geometrical nonlinear simulation and does not require advanced failure mechanics implementation. However, the failure evolution and series of events clearly demonstrates the importance of geometrically nonlinear simulations. Linear elastic simulations would not reveal the series of events and its consequences.

The presented model was subjected to some restrictions, which may influence the final blade failure prediction. Firstly, progressive damage growth was only implemented for elements on the pressure side and not applied to the blade suction side. The limitation was made in order to save computational time and because the damage on the suction side was considered to be neglectable. Furthermore, crack growth in the trailing edge was limited to crack growth in the middle of the bondline.

This work showed explicitly how the combined load led to trailing edge buckle at early load levels and clearly visible at a load level of approximately 75%. Strongly connected to the buckling wave was the significantly increase of the energy release rate at trailing edge joint. Surprisingly, at load levels

below the design load level the buckling wave initially occurred and had strong impact on the occurring energy release rates. Further investigation will be undertaken to investigate that in more detail.

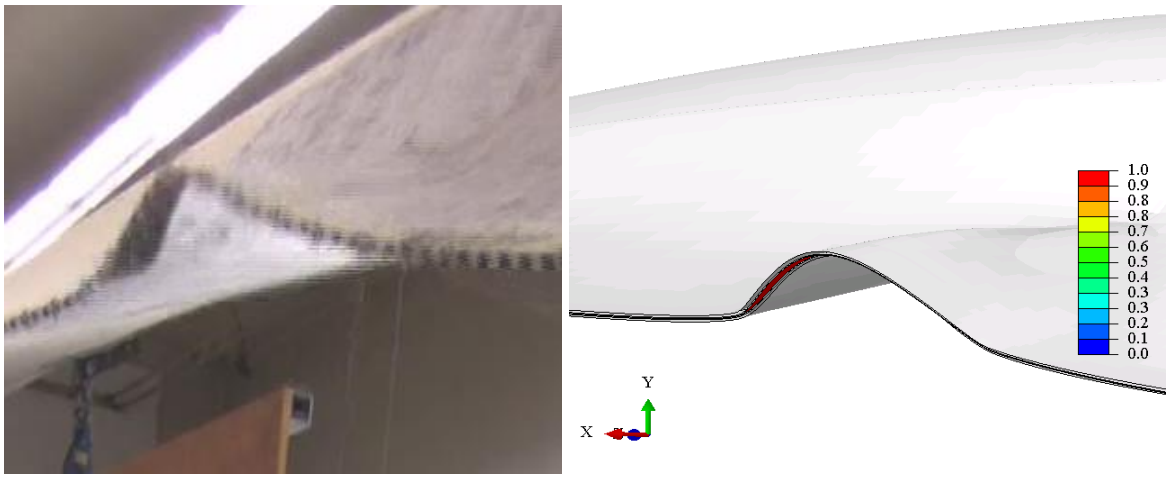

Figure 12: (a) Sudden trailing edge opening initiating blade collapse. (b) Numerical simulation and trailing edge opening (scaled with a factor 2).

ACKNOWLEDGEMENTS

The work is supported by the new Danish Centre for Composite Structures and Materials for Wind Turbines (DCCSM), grant no. 09-067212 form the Danish Strategic Research Council. The support is gratefully acknowledged. The work is furthermore based on “Exerpimental Blade Research – Phase 2” results friendly supported by the Danish Energy Agency through the 2010 Energy Technology Development and Demonstration Program (EUDP).

The authors wish to thank especially Martin A. Eder and Federico Belloni for conducting the experimental blade test and kindly providing the experimental data. Moreover, the authors are grateful for help from the Aeroelastic Design group at DTU Wind Energy supporting the aero-elastic calculation significantly.

REFERENCES

[1] S. Sheng, Report on Wind Turbine Subsystem Reliability - A survey of Various Databases, Tech. rep., NREL/PR-5000-59111 (2013).

[2] S. Ataya and M. M. Z. Ahmed, Damages of Wind Turbine Blade Trailing Edge: Forms, Location, and Root Causes, Journal of Engineering Failure Analysis 35 (2013) 480–488.

[3] R. D. Bitsche, F. Belloni and M. A. Eder Effects of geometric non-linearity on energy release rates in a realistic wind turbine blade cross section, submitted in 2015

[4] M. A. Eder and R. D. Bitsche, A qualitative analytical investigation of geometrically nonlinear effects in wind turbine blade cross sections, Thin-Walled Structures 93 (2015) 1–9.

[5] P. U. Haselbach, F. Belloni and M. A. Eder, A holistic investigation of trailing edge damage in a wind turbine rotor blade, submitted in 2015

[6] M. A. Eder and R. D. Bitsche, Fracture analysis of adhesive joints in wind turbine blades, Wind Energy (2014) 16.

[7] J. P. Blasques, User´s manual for BECAS - a cross section analysis tool for anisotropic and inhomogeneous beam sections of arbitrary geometry, Tech. Rep. Riso-R-1785(EN), Risø DTU, National Laboratory for Sustainable Energy (2011).

[8] T. Kim, A. M. Hansen, K. Branner, Development of an anisotropic beam finite element for composite wind turbine blades in multibody system, Renewable Energy, 2013

[9] Larsen, T. J. and Hansen, A. M., How 2 HAWC2, the user´s manual, Risø-R-1576(ver.4-5)(EN)
[10] IEC 61400-1 International Standard: Wind turbines - Part 1: Design requirements, Edition 3.0. 2010-10.
[11] http://www.hawcstab2.vindenergi.dtu.dk/
[12] Abaqus, 2015 Dassault System. Abaqus Analysis User Manual, Vol. 6.13
[13] Hashin, Z., "Failure Criteria for Unidirectional Fiber Composites," Journal of Applied Mechanics, vol. 47, pp. 329–334, 1980.
[14] Hashin, Z. and A. Rotem,, A Fatigue Criterion for Fiber-Reinforced Materials, Journal of Composite Materials, vol. 7, pp. 448–464, 1973.
[15] Lapczyk, I., and J. A. Hurtado, Progressive Damage Modeling in Fiber-Reinforced Materials, Composites Part A: Applied Science and Manufacturing, vol. 38, no.11, pp. 2333–2341, 2007.
[16] Matzenmiller, A., J. Lubliner, and R. L. Taylor, A Constitutive Model for Anisotropic Damage in Fiber-Composites, Mechanics of Materials, vol. 20, pp. 125–152, 1995.
[17] Benzeggagh, M. L. and M. Kenane, Measurement of Mixed-Mode Delamination Fracture Toughness of Unidirectional Glass/Epoxy Composites with Mixed-Mode Bending Apparatus, Composites Science and Technology, vol. 56, pp. 439–449, 1996.
[18] Camanho, P. P., and C. G. Davila, Mixed-Mode Decohesion Finite Elements for the Simulation of Delamination in Composite Materials,NASA/TM-2002–211737, pp. 1–37, 2002.
[19] Krueger, R. The Virtual Crack Closure Technique: History, Approach 570 and Applications NASA Langley Research Center in Hampton, Institute for Computer Applications in Science & Engineering (ICASE),2002, 572 ICASE Report No. 2002-10.
[20] F. Lahuerta, T. Westphal, R. P. L. Nijssen, F. P. van der Meer and L. J. Sluys, Stattic and Fatique performance of thick laminates test design and experimental compression results, ECCM-16th, Seville, Spain, 2014.
[21] D Zenkert (Editor), Handbook of Sandwich Construction, Engineering Materials Advisory Services Ltd., 1997
[22] T. C. Triantafillou and L. J. Gibson, Failure Mode Maps for Foam Core Sandwich Beams. Material Science and Engineering, 95 (1987), 37-53.